

## Polarimetry of the eclipsing pulsar PSR J1748–2446A

X. P. YOU,<sup>1</sup> R. N. MANCHESTER,<sup>2</sup> W. A. COLES,<sup>3</sup> G. B. HOBBS,<sup>2</sup> AND R. SHANNON<sup>4</sup>

<sup>1</sup>*School of Physical Science and Technology, Southwest University, Chongqing 400715, China*

<sup>2</sup>*CSIRO Astronomy and Space Science, PO Box 76, Epping, NSW 1710, Australia*

<sup>3</sup>*Electrical and Computer Engineering, University of California at San Diego, La Jolla, California 92093, USA*

<sup>4</sup>*Centre for Astrophysics and Supercomputing, Swinburne University of Technology, Hawthorn, VIC 3122, Australia*

### ABSTRACT

Observations with the Parkes radio telescope of the eclipsing millisecond binary pulsar PSR J1748–2446A, which is in the globular cluster Terzan 5, are presented. These include the first observations of this pulsar in the 3 GHz frequency band, along with simultaneous observations in the 700 MHz band and new observations around 1400 MHz. We show that the pulsar signal is not eclipsed in the 3 GHz band and observe the known eclipses in the lower frequency bands. We find that the observed pulse signal becomes depolarized during particular orbital phases and postulate that this depolarization occurs because of rotation-measure fluctuations resulting from turbulence in the stellar wind responsible for the eclipses.

*Keywords:* binaries: eclipsing - polarization - pulsars: individual (PSR J1748–2446A)

### 1. INTRODUCTION

The pulsar PSR J1748–2446A (PSR B1744–24A) was discovered by Lyne et al. (1990) using the 64-m diameter Parkes radio telescope. This was the second known binary pulsar system for which the pulsed signal is eclipsed during part of the orbit and it is the prototype for the class of eclipsing binary pulsars now known as “redbacks” (Roberts 2013). The pulsar has a pulse period of 11.56 ms and is located within the globular cluster Terzan 5 (hence also known as Ter 5A) and is in a low-eccentricity orbit with an orbital period of only 109 minutes. The companion mass is estimated to be at least  $0.089M_{\odot}$ . The projected semi-major axis of this system (0.12 light seconds) implies that the separation between the pulsar and its white dwarf companion is around  $0.85R_{\odot}$ .

The duration of the eclipse is variable in time and also changes as a function of the observing frequency. In the 20 cm (1.4 GHz) observing band the eclipse duration is more than one-third of the orbital period (Lyne et al. 1990). The expected eclipse duration due to a Roche lobe of estimated radius  $0.15R_{\odot}$  (Nice & Thorsett 1992) is only six minutes, much less than the typical eclipse duration. Therefore, the eclipse must be caused by an ablated wind from the companion. Nice et al. (1990) observed the pulsar at frequencies between 0.8 and 1.66 GHz and found that the eclipse duration decreases with observing frequency  $\nu$  with a dependence of  $\nu^{-0.63\pm 0.18}$ .

Understanding the eclipse mechanism can provide the opportunity to probe the mechanism of the pulsar radiation and also the interaction between the pulsar wind and the companion. There have been many attempts to explain the eclipse mechanism, for example, refractive effects (Phinney et al. 1988), pulse smearing (Ryba & Taylor 1991), cyclotron and synchrotron absorption (Eichler 1991; Thompson et al. 1994), induced scattering (Luo & Melrose 1995) and free-free absorption (Wasserman & Cordes 1988; Rasio et al. 1989, 1991). However, the published mechanisms based on refraction cannot explain the frequency dependence of the eclipse duration. Pulse smearing models requires a longer dispersion time delay near the eclipse than is observed (Nice et al. 1990). Cyclotron and synchrotron absorption models require very high magnetic fields and pulsar winds that are much hotter than is usually assumed (Thompson et al. 1994). Free-free absorption can explain the dependence between the eclipse duration and the observing frequencies and currently seems consistent with observations, although it does require a relatively low wind temperature (Fruchter & Goss 1992).

In this paper, we present multi-frequency observations of PSR J1748–2446A made with the Parkes 64-m radio telescope. Our observations and analysis methods are described in Section 2. In Section 3 we investigate how the pulsar’s polarization properties and its rotation measure (RM) vary as function of orbital phase and we discuss the implications of this work in Section 3.3. We summarize our conclusions in Section 5.

After completing most of this work, we became aware that Anna Bilous in her PhD thesis (Bilous 2012) had also observed the orbital-phase dependence of polarization for PSR J1748–2446A in bands centered at 820 MHz and 1500 MHz using the Green Bank Telescope. Her results show a similar radio-frequency and orbital-phase dependence for the linear polarisation to those presented here. She also attributed the linear depolarization to RM fluctuations in the circumstellar plasma.

## 2. OBSERVATION AND DATA ANALYSIS

Our observations were made between November 2014 and January 2015, using the Parkes 64-m diameter radio telescope. The data were taken in three frequency bands which we label 40 cm, 20 cm and 10 cm, centered at 728 MHz, 1369 MHz and 3100 MHz, respectively. In the 20 cm band the central beam of the multibeam receiver was used. Observations in the 10 cm and 40 cm bands were simultaneous and used the dual-band 10 cm/50 cm receiver. We recorded a bandwidth of 64 MHz at 40 cm, 256 MHz at 20 cm and 1024 MHz at 10 cm, divided into 128, 1024 and 1024 frequency channels for the three bands respectively. The signal processing systems used were the Parkes digital filterband system, PDFB4, for the 20 cm and 10 cm observations, and a coherent dedispersion system, CASPSR (van Straten & Bailes 2011), for the 40 cm observations. All of the data were recorded in full polarization mode with 1-min subintegrations. Before each observations of the pulsar, a 2-min pulsed calibration signal was recorded. We used measurements of Hydra A to calibrate the flux density scale for our pulsar observations.

All the observations were initially processed and calibrated using PSRCHIVE (Hotan et al. 2004). In brief, we removed 5% of the band-edges along with narrow band interference. We then calibrated our observations using the polarisation and flux density calibrators. The 20 cm observations are affected by cross-coupling within the feed. We used the PCM method to account for this cross-coupling (van Straten 2004).

We aim to investigate the properties of the pulsar as function of orbital phase. We therefore obtained relatively high signal-to-noise ratio (S/N) polarization profiles at a range of orbital phases by forming profiles for every 3 minutes of observing time. To form the mean polarization profiles, the

Faraday rotation across the observing band must be taken into account. Since the rotation measure (RM) could vary as a function of orbital phase, we measured the RM for each 3-minute profile using the PSRCHIVE routine RMFIT. We initially searched over a large range in RM (from  $-1000$  to  $1000 \text{ rad m}^{-2}$ ) and determined the RM which maximized the linearly polarized intensity. To improve on this estimate the total observing band was divided into two parts and the RM value was used to sum the polarization profile in each half. The final RM value was then obtained by calculating the weighted mean position angle difference between the two bands and, if necessary, iterating.

### 3. RESULTS

#### 3.1. Variation of flux density with orbital phase

The mean pulsed flux density ( $S$ ) as function of orbital phase for the three observing bands is presented in Figure 1 with the independent observations shown in different colors. It is clear that the duration of the eclipse decreases with increasing observation frequency as already found by Lyne et al. (1990) and Nice et al. (1990). We find no evidence of any eclipse in the 10 cm band (bottom panel of Figure 1) although the observed flux density is quite variable at all orbital phases.

Although Lyne et al. (1990) found the eclipse durations to be variable, the eclipses we observed in a given band were similar in length. Figure 1 shows that the rate of egress from the eclipse (around orbital phase 0.5) was significantly quicker than the rate of ingress (around orbital phase 1.0) for both 20 cm and 40 cm. We quantified this by approximating the egress and ingress as linear changes and measuring the phase interval between zero and maximum flux density (or vice versa). For the 20 cm band, the rate of egress is variable, with phase intervals of about 0.10 for two days (blue and green in Figure 1) and 0.20 for the other day (red). The rate of ingress was slower, but more stable with the interval for all days being close to 0.21. For 40 cm, only one egress and one ingress is measurable, with intervals of about 0.09 and 0.16, respectively. A similar pattern of slow ingress and more rapid egress is seen in other eclipsing systems, e.g., PSR B1975+20 (Ryba & Taylor 1991).

#### 3.2. Polarization profiles

To measure the mean profile polarization in each band, we used the following procedure. We first measured the RM for every 3-minute profile. As will be discussed further in Section 3.3 below, we found that the RM was measurable only for profiles in the central part of the non-eclipsed phase at 20 cm and 40 cm. The RM was found to be stable throughout these central phase ranges and so we were able to sum those 3-minute profiles to form a high S/N profile for each band as shown in Figure 2. We then redetermined the RM using these summed profiles, obtaining values of  $186.4 \pm 6.2 \text{ rad m}^{-2}$  at 40 cm and  $174.9 \pm 4.2 \text{ rad m}^{-2}$  at 20 cm. These two values are consistent within their uncertainties. The weighted mean RM,  $178.5 \pm 3.5 \text{ rad m}^{-2}$ , was used to make the plots shown in Figure 2.

It is evident that the pulse total intensity profiles evolve strongly across the three bands with a prominent leading component seen at 10 cm. The relative alignment of the profiles in pulse phase is somewhat uncertain, but the circular polarization profiles suggest that the main component at 10 cm aligns with the main component at the two lower bands. It is likely that some of the signal on the trailing edge of the 40 cm profile results from interstellar scattering (cf., Nice & Thorsett 1992). Never-the-less, it appears that the leading part of the profile has a flatter spectrum than the trailing part.

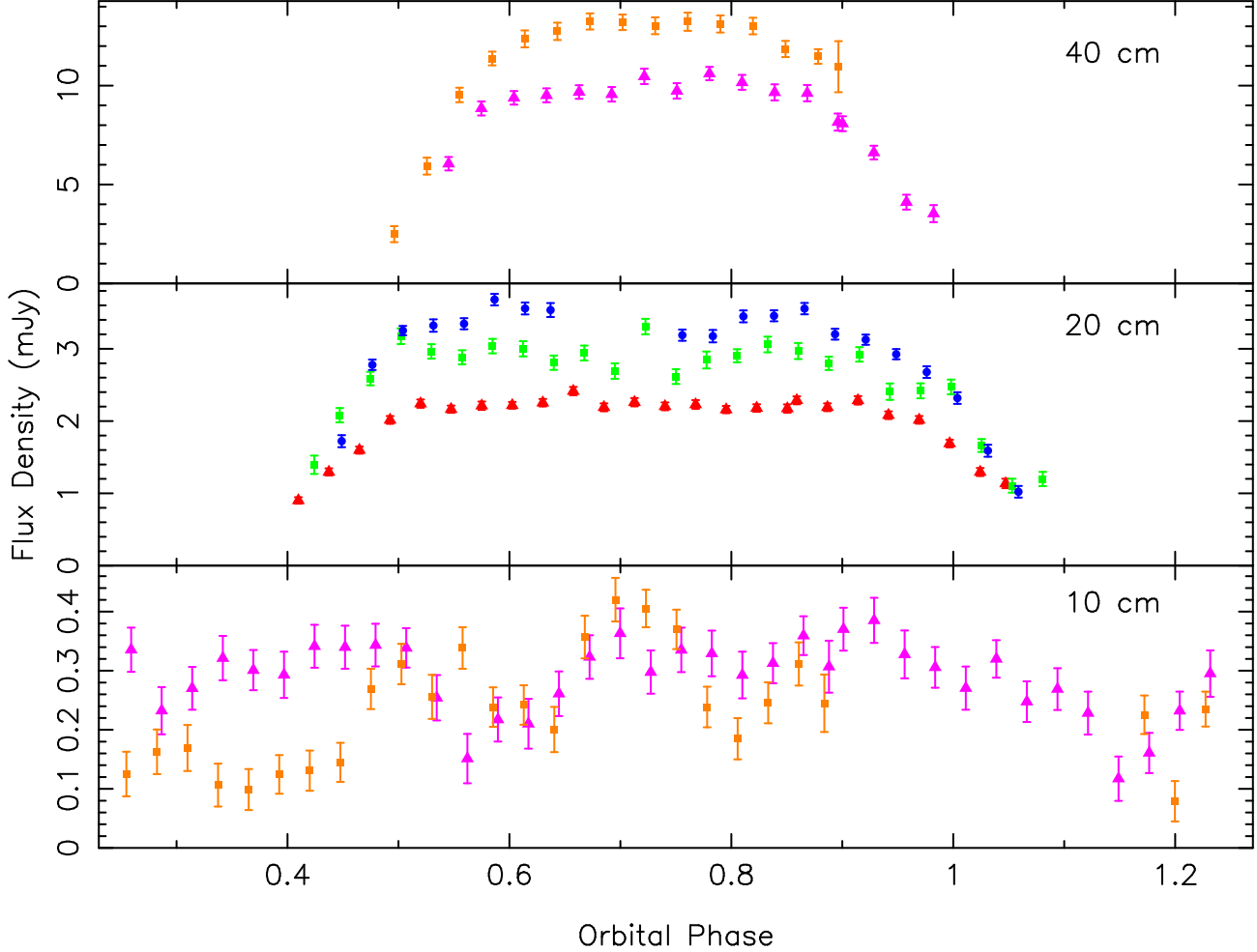


**Figure 1.** Mean pulse flux density as a function of orbital phase. The upper, middle and lower panels show the results for observations at 40 cm, 20 cm, and 10 cm respectively, with different colors representing different observation dates. Observations were made simultaneously in the 10 cm and 40 cm bands and so we use the same color for these two bands. Observation dates (MJD) were: red: 56973.27, green: 57003.92, blue: 57007.21, purple: 57032.12, orange: 57041.14, Note that for two observations there are some missing points corresponding to gaps in the observations (blue: phases 0.63 - 0.75, orange: phases 0.9 - 1.17).

We did not detect any linear polarization at any orbital phase for the 10 cm band, either using the 3-minute profiles or using the summation of all the observations. Since we see no evidence for an eclipse in this band, the low level of linear polarization at 10 cm or 3 GHz is likely to be intrinsic to the emission mechanism. For all three observing bands we measure significant circular polarization (shown with a blue line in the Figure) with a similar variation across the profile in all three bands, although at 10 cm the leading positive peak is barely significant.

Since the position angles in Figure 2 are calibrated according to the IAU convention (van Straten et al. 2010) and the pulse profiles and PA variations across the 40 cm and 20 cm profiles are similar and relatively flat, we can use the weighted mean position angle difference between these bands to obtain an improved estimate of the RM. The derived value is  $181.2 \pm 0.5 \text{ rad m}^{-2}$ . The small differences in the form of PA variations across the 40 cm and 20 cm profiles almost certainly are intrinsic to the

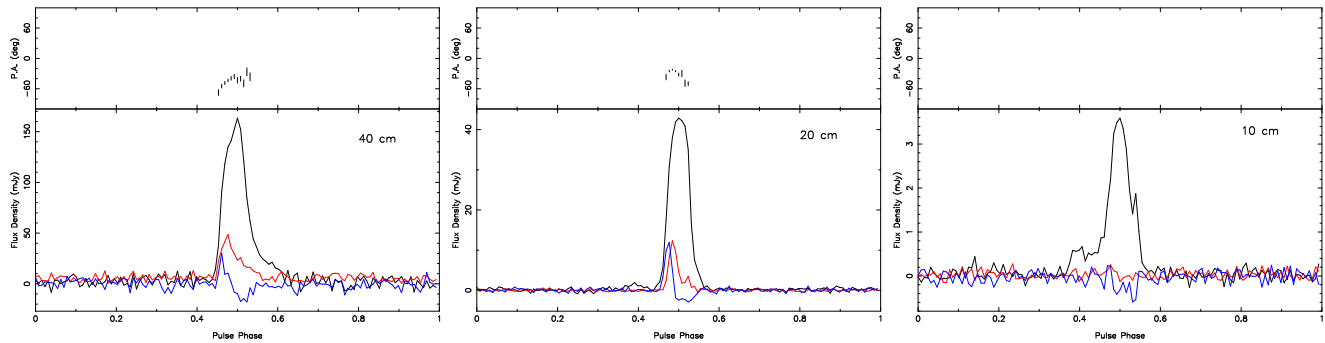


**Figure 2.** Mean pulse polarization profiles of PSR J1748–2446A in the 40 cm, 20 cm and 10 cm observing bands. The lower panels give the total intensity (Stokes  $I$ , black line), linearly polarized intensity ( $L = (Q^2 + U^2)^{1/2}$ , where  $Q$  and  $U$  are the linear Stokes parameters, red line) and circularly polarized intensity (Stokes  $V = I_{\text{LH}} - I_{\text{RH}}$ , blue line) (cf. van Straten et al. 2010). The upper panels give the position angle of the linear polarization. Profile alignment is not absolute; the profile peaks are simply placed at pulse phase 0.5.

pulse emission, but never-the-less result in a small variation in apparent RM across the profile. The quoted uncertainty on the mean RM includes the effect of this variation.

### 3.3. Depolarization

Figure 3 shows the variation of pulsed flux density, mean fractional linear polarization and RM as a function of orbital phase for the 40 cm and 20 cm bands. We can divide the orbit into three zones: a) when the pulse is fully eclipsed, b) when the pulse is detectable but unpolarized and c) when the pulse is detectable and significantly linearly polarized. As discussed above, we see no eclipse nor any significant linear polarization for the 10 cm-band data.

The well-known frequency dependence of the eclipse duration is evident from the bottom panels. The middle panels show that phase c), when significant linear polarization is detected, is concentrated in the middle of the un-eclipsed region and is of significantly shorter duration than the un-eclipsed phase. Consequently, there are zones of type b), that is, detectable pulses with no significant linear polarization, on either side of the type c) zone. The duration of zone c) is about 12 minutes (0.11 in phase) at 40 cm and 33 minutes (0.30 in phase) at 20 cm. Zone b) is wider on ingress to the eclipse (around phase 1.0) at both 20 cm and 40 cm, but has a total duration (sum of egress and ingress zones) that is similar for the two bands, about 40 minutes or 0.37 in phase.

We determine the RM variations shown in the top panel of Figure 3 by comparing the average position angle

$$\psi_{\text{av}} = 0.5 \tan^{-1} \frac{\langle U \rangle}{\langle Q \rangle}, \quad (1)$$

of each 3-minute profile having significant linear polarization with the average position angle of the mean profile shown in Figure 2. The Stokes parameters in Equation 1 are averaged over the part of the pulse profile with significant  $L$ . When the linear polarization is significant (zone c), the RM is relatively stable.

## 4. DISCUSSION

### 4.1. Eclipse duration

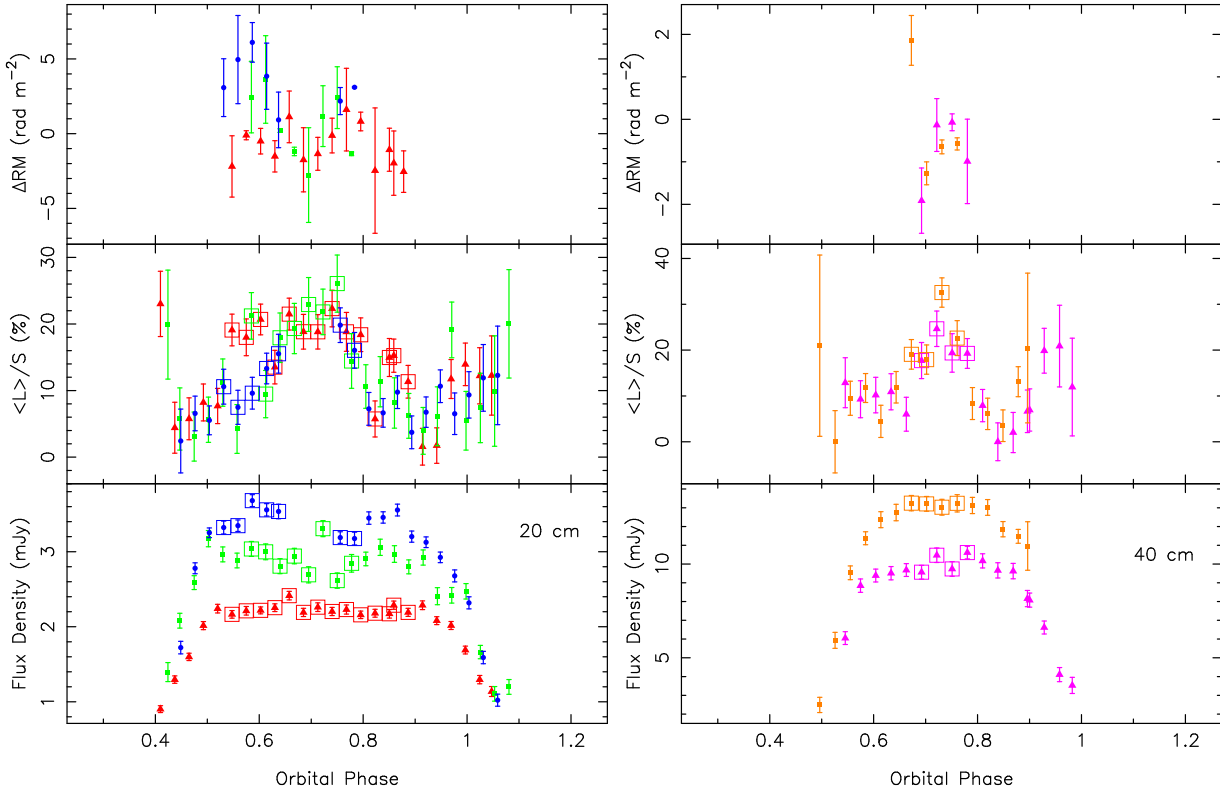


**Figure 3.** Polarization properties of PSR J1748–2446A at 20 cm and 40 cm as a function of orbital phase. The bottom panels for each band show the pulse mean flux density for each observing frequency as a function of orbital phase. As in Figure 1, the different colours represent different observation dates. The middle panels show the mean fractional linear polarization  $\langle L \rangle / S$ , where  $L = \sqrt{Q^2 + U^2}$  and  $Q$  and  $U$  are the linear Stokes parameters. Since  $L$  is a positive-definite quantity, it has a non-zero mean from system noise even when the pulse is effectively unpolarized. Points marked with squares indicate that the pulse is significantly linearly polarized at that orbital phase. The upper panels show the RM variations based on position angle differences relative to the mean profiles shown in Figure 2.

The eclipse durations at 20 cm and 40 cm illustrated in Figures 1 and 3 are about 32% and 50% of the orbital period, consistent with previous results (Nice et al. 1990; Thorsett & Nice 1991). These observed durations give a frequency dependence  $\sim \nu^{-0.71 \pm 0.15}$ . This is consistent with the  $\nu^{-0.63 \pm 0.18}$  dependence derived by Nice et al. (1990). However, if we extrapolate this result to the 10 cm observing band then the eclipse duration would be about 0.18 of the orbital period or about 20 minutes. This would easily be detectable, but we do not see any evidence for such an eclipse. Our observing bands do not provide sufficient coverage to determine the frequency at which the eclipse becomes undetectable, but it certainly occurs between 1.6 GHz (Nice et al. 1990) and 2.6 GHz, the lower edge of our 10 cm band.

Although no eclipses are seen at 10 cm, Figure 1 shows considerable variability across all orbital phases in the observed flux density. The lack of dependence on orbital phase suggests that this variability is not related to the circumstellar gas. It is more likely to result from diffractive interstellar scintillation.

#### 4.2. Depolarization mechanism

As Figure 3 shows, the pulsar pulse is depolarized around the boundaries of the eclipse, with the depolarization more pronounced in the 40 cm band compared to the 20 cm band. The most likely cause of this depolarization is multi-path propagation in the circumstellar magnetised plasma leading to rapid time variations in the RM, although the traversal of the line of sight through the circumstellar plasma due to orbital motion will also contribute. Such rapid RM variations can result from fluctuations in either or both of the circumstellar component of DM and the parallel component of the magnetic field. DM variations are observed at both eclipse ingress and egress, with those at egress generally more significant (Ryba & Taylor 1991; Nice & Thorsett 1992). However, these variations are typically  $\lesssim 0.1 \text{ cm}^{-3} \text{ pc}$  which will not significantly affect the RM. There is weak evidence for broadening of the mean pulse profiles at eclipse ingress or egress relative to the uneclipsed profile at the 10% level by  $\lesssim 0.5 \text{ ms}$ , corresponding to a  $\Delta\text{DM} \lesssim 0.2 \text{ cm}^{-3} \text{ pc}$ . Consequently DM fluctuations are unlikely to be responsible for the depolarization. Therefore small-scale variations in the line-of-sight component of the magnetic field are the most likely cause of the depolarization, irrespective of whether the RM variations result from multi-path propagation or orbital motion of the line of sight. Such fluctuations would be expected in a turbulent stellar wind.

If the RM variations have a normal distribution with standard deviation  $\sigma_{\text{RM}}$ , the variations in polarization position angle  $\psi$  will also be normal with standard deviation  $\sigma_{\psi} = \lambda^2 \sigma_{\text{RM}}$ . Averaging over this variation will reduce the linear polarization  $L$  by a factor  $\exp(-2\sigma_{\psi}^2) = \exp(-2\lambda^4 \sigma_{\text{RM}}^2)$  (see Appendix A).

As expected and as observed, the depolarization mechanism is more effective at longer wavelengths. If we assume that the depolarization is significant when  $\sigma_{\text{RM}}^2 \lambda^4 > 1$ , then depolarization will occur if  $\sigma_{\text{RM}}$  is greater than  $6 \text{ rad m}^{-2}$  at 40 cm,  $25 \text{ rad m}^{-2}$  at 20 cm and  $100 \text{ rad m}^{-2}$  at 10 cm respectively. Figure 3 shows that, at orbital phases from about 0.55 and 0.67 and from 0.78 to 0.90 (when the pulsar – companion line is between  $20^\circ$  and  $63^\circ$  from the line of sight) the pulse is depolarized at 40 cm but not at 20 cm. Consequently at these orbital phases,  $\sigma_{\text{RM}}$  must be between  $6 \text{ rad m}^{-2}$  and  $25 \text{ rad m}^{-2}$ . The top panel of Figure 3 shows RM fluctuations of this order. For a fluctuating electron density of order  $10^6 \text{ cm}^{-3}$  (Rasio et al. 1991) and a path length of order  $1 R_{\odot}$ , the implied magnetic field is of order  $10 \mu\text{G}$  which is plausible. More detailed modelling would require three-dimensional models of both the circumstellar plasma and the magnetic field structure.

## 5. CONCLUSIONS

Polarization observations of the eclipsing binary pulsar J1748–2446A, the first-discovered pulsar in the globular cluster Terzan 5, have been made in three bands using the Parkes 64-m radio telescope: 40 cm (centered at 728 MHz), 20 cm (1369 MHz) and, for the first time, at 10 cm (3100 MHz). Observations in the two lower-frequency bands show the well-known eclipses, but no eclipses are evident at 10 cm. Away from the eclipses, the two lower-frequency bands show significant linear and circular polarization, but at 10 cm, there is no detectable linear polarization. As the pulsar enters and leaves the eclipse, the linear polarization at 20 cm and 40 cm is quenched. We attribute this depolarization to short-timescale RM fluctuations caused by time-variable scattering and the resultant multi-path propagation in the circumstellar plasma, and to the changing propagation path due to orbital motion. An ultra-wide-bandwidth receiver, currently being commissioned at the Parkes radio telescope, will have increased sensitivity and frequency coverage compared to the current receivers. This new receiver will be ideal for carrying out further studies of this pulsar and the orbital dependence of its polarization.

## ACKNOWLEDGMENTS

Our initial observations were based on a timing model for PSR J1748–2446A provided by S. M. Ransom and obtained using the Green Bank radio telescope. XPY is supported by the National Natural Science Foundation of China (U1231120, 11573008) and the Fundamental Research Funds for the Central Universities (XDJK2015B012). GH is supported by an Australian Research Council Future Fellowship grant. The data presented in this paper were obtained by the Parkes radio telescope, which is part of the Australia Telescope which is funded by the Commonwealth of Australia for operation as a National Facility managed by CSIRO.

*Software:* psrchive(Hotan et al. 2004), <https://sourceforge.net/projects/psrchive/>, version 2012-09+

## REFERENCES

- Bilous, A. 2012, PhD thesis, University of Virginia
- Born, M. & Wolf, E. 1970, Principles of Optics, Cambridge Press
- Eichler, D. 1991, ApJ, 370, L27
- Fruchter, A. S. & Goss, W. M. 1992, ApJ, 384, L47
- Hotan, A. W., van Straten, W., & Manchester, R. N. 2004, PASA, 21, 302
- Luo, Q. & Melrose, D. M. 1995, ApJ, 452, 346
- Lyne, A. G., Manchester, R. N., D’Amico, N., Staveley-Smith, L., Johnston, S., Lim, J., Fruchter, A. S., Goss, W. M., & Frail, D. 1990, Nature, 347, 650
- Nice, D. J. & Thorsett, S. E. 1992, ApJ, 397, 249
- Nice, D. J., Thorsett, S. E., Taylor, J. H., & Fruchter, A. S. 1990, ApJ, 361, L61
- Papoulis, A. 1991, Probability, Random Variables, and Stochastic Processes, McGraw Hill
- Phinney, E. S., Evans, C. R., Blandford, R. D., & Kulkarni, S. R. 1988, Nature, 333, 832
- Rasio, F. A., Shapiro, S. L., & Teukolsky, S. A. 1989, ApJ, 342, 934
- . 1991, A&A, 241, L25
- Roberts, M. S. E. 2013, in IAU Symposium, Vol. 291, Neutron Stars and Pulsars: Challenges and Opportunities after 80 years, ed. J. van Leeuwen, 127–132
- Ryba, M. F. & Taylor, J. H. 1991, ApJ, 380, 557
- Thompson, C., Blandford, R. D., Evans, C. R., & Phinney, E. S. 1994, ApJ, 422, 304
- Thorsett, S. E. & Nice, D. J. 1991, Nature, 353, 731
- van Straten, W. 2004, ApJS, 152, 129
- van Straten, W. & Bailes, M. 2011, PASA, 28, 1
- van Straten, W., Manchester, R. N., Johnston, S., & Reynolds, J. E. 2010, PASA, 27, 104
- Wasserman, I. & Cordes, J. M. 1988, ApJ, 333, L91



## APPENDIX

## A. DERIVATION OF DEPOLARIZATION FACTOR

Any partial coherence such as depolarization or reduction in visibility of an interferometer, requires both finite bandwidth and finite integration time (Born & Wolf 1970). Partial polarization can be described by coherency matrix  $\mathbf{C} = \mathbf{E}\mathbf{E}^T$  where the 2-vector  $\mathbf{E}$  components are any two orthogonal polarizations. Here we take a linear basis. We then consider the effect of multi-path propagation on a unit amplitude wave polarized in the x direction. The different paths have different Faraday rotation angle  $\psi$ . Then  $\mathbf{C}$  becomes

$$\mathbf{C} = \begin{bmatrix} \cos^2 \psi & -\cos \psi \sin \psi \\ -\cos \psi \sin \psi & \sin^2 \psi \end{bmatrix}. \quad (\text{A1})$$

We assume  $\psi$  to be a zero mean gaussian random variable and take the expectation of  $\mathbf{C}$  over paths, thus explicitly over  $\psi$  and implicitly over time. The expectations of the off diagonal terms  $C_{xy}$  and  $C_{yx}$  are zero as  $\psi$  has an even distribution. The diagonal terms can be written

$$\begin{aligned} \langle C_{xx} \rangle &= \langle \cos^2 \psi \rangle = 0.5(1 + \langle \cos 2\psi \rangle) \\ \langle C_{yy} \rangle &= \langle \sin^2 \psi \rangle = 0.5(1 - \langle \cos 2\psi \rangle). \end{aligned} \quad (\text{A2})$$

$\langle \mathbf{C} \rangle$  can be written as the sum of an unpolarized component  $\langle \mathbf{C}_{\text{up}} \rangle$  and a 100% linearly polarized x-component  $\langle \mathbf{C}_{\text{p}} \rangle$  where

$$\langle \mathbf{C}_{\text{up}} \rangle = \begin{bmatrix} \langle C_{yy} \rangle & 0 \\ 0 & \langle C_{yy} \rangle \end{bmatrix}, \quad \langle \mathbf{C}_{\text{p}} \rangle = \begin{bmatrix} \langle C_{xx} \rangle - \langle C_{yy} \rangle & 0 \\ 0 & 0 \end{bmatrix}. \quad (\text{A3})$$

Thus the amplitude of the linear polarized component has been reduced from 1.0 to

$$L = \langle C_{xx} \rangle - \langle C_{yy} \rangle = \langle \cos 2\psi \rangle = \exp(-2\sigma_\psi^2) \quad (\text{A4})$$

where the latter equality is applicable for normal random processes (Papoulis, A. 1991).